ORIGINAL ARTICLE

A case study of debris flow risk assessment and hazard range prediction based on a neural network algorithm and finite volume shallow water flow model

Yuchao Li[1] · Jianping Chen[1] · Zhihai Li[1] · Xudong Han[2] · Shijie Zhai[1] · Yongchao Li[1] · Yiwei Zhang[1]

Abstract

Due to the need of economic development and energy structure adjustment, China intends to build a number of pumped storage power stations for hydroelectric storage to generate electricity. Pumped storage power stations are generally built in mountainous or hilly areas where sufficient water and height differences will provide the adequate head difference. Geological processes, such as debris flows, often occur in mountainous areas and are one of the main threats to power stations and related projects. In this work, the debris flows in the engineering area of a pumped storage power station in Shangyi County, Hebei Province were selected as a case study. The neural network model was adopted to quantitatively calculate the probability of debris flows. Then, risk zoning was implemented according to the probability values. Finally, the debris flow numerical simulation software SFLOW, which is based on the finite volume shallow water flow model, was used for high-risk gullies. The spatial hazard range of each debris flow was predicted for rainfall frequencies of 20, 50, 100, and 200 years. And the sensitivity of parameters affecting debris flow migration and the advantages of SFLOW compared with FLO-2D software were discussed. In general, the SFLOW model can accurately and efficiently solve the problem of fluid flow on irregular terrain and can be applied to similar engineering projects.

Keywords Pumped storage power stations · Waste slag bodies · Debris flow · Risk assessment · Numerical simulation

Introduction

Some of the traditional, non-renewable energy sources are gradually being depleted in China due to the exponential increase in industrial and residential development (Lai et al. 2019; Valero and Valero 2010). In response, the value of utilizing renewable energy has been consistently emphasized. In recent years, hydropower has been one of the primary energy sources harvested in China, due to its being both clean and renewable. Because southwest China is the main source of large rivers, many large hydropower projects have been established or are under construction (Zhan et al. 2018) in the region. For cities with relatively scarce water

resources, a new hydropower station, known as a pumped storage power station, has become a new option. Pumped storage power stations use electrical energy to pump water to the upper reservoir when the power supply demand is low and then discharges water to the lower reservoir when the power supply demand is high (Bao et al. 2019b). However, pumped storage power stations are generally built in mountainous or hilly areas to obtain the necessary water quantity and height differences. Therefore, the debris flows that easily occur in mountainous areas threaten the safety of these hydropower engineering projects. Over the last few decades, significant damage to lives, infrastructure, and property has been caused by debris flows in mountainous areas (Chang et al. 2017; Chen et al. 2018; Huang et al. 2014; Meng and Wang 2015). Therefore, analyzing and evaluating the risk of debris flows in the study area as well as forecasting the extent of damage is of maximum importance. However, quantitative evaluation of debris flows is difficult, as they are complex, nonlinear geological phenomena. Currently, research on the susceptibility, sensitivity (Dong et al. 2009), and risk of debris flows (Liu 2002; Gentile et al. 2007) are

✉ Jianping Chen
   chenjpwq@126.com

1 College of Construction Engineering, Jilin University, Changchun 130026, China

2 Center for Hydrogeology and Environmental Geology, CGS, Baoding 071501, China

important directions to the study of debris flow spatial forecasting. In particular, the influence factor (Lin et al. 2002) and the selection of evaluation methods are key issues. The selection of factors is related to the assessment content—mainly topography, meteorology, hydrology, soil vegetation, human activities, and debris flow history parameters. From a methodology perspective, quantitative and semi-quantitative, linear and nonlinear mathematical-statistical methods are primarily used in the evaluation—such as the analytic hierarchy process (Wu et al. 2016), logistic regression method (Regmi et al. 2013; Tunusluoglu et al. 2007), support vector machine (Wang et al. 2016a), neural network (Lee et al. 2003; Liu et al. 2005) and Bayesian network algorithm (Liang et al. 2012; Tien Bui et al. 2012), etc. These methods have corresponding advantages and limitations for research subjects with different geological conditions. However, the risk assessment alone cannot meet the needs of debris flow prevention. Therefore, the simulation of debris flows dynamic process and the prediction of hazard range are important links in debris flow evaluation.

With the continuous maturity of computer technology, a significant variety of numerical methods have been applied to the study of debris flows— e.g., shallow water flow model (SWM) (Lin et al. 2001), smooth particle hydrodynamics method (SPH) (Wang et al. 2016b; Huang et al. 2014), discrete element method (DEM) (Bao et al. 2019a), discontinuous deformation analysis (DDA), multiphase fluid–solid coupling model (Bout et al. 2018), etc. Among them, the SWM is widely used because it can effectively reflect the fluid's physical properties and has a high computational efficiency. The shallow water equation obtained by integrating Navier–Stokes equation in the vertical direction can describe the fluid characteristics in large-scale space without occupying too much computer space. In order to solve shallow water equations, many methods such as the finite difference method, finite element method and finite volume method have been developed. Compared with the other two methods, the finite volume method can not only ensure the balance between water quantity and momentum but also maintain high computational performance in any computational domain. The SFLOW software was developed by Han (Han et al. 2017, 2018) based on Godunov-type finite volume shallow water model. SFLOW ensures the conservation of water volume and momentum and allows the processing of complex terrain data. The model not only considers the friction and viscosity properties but also the solid particle contact energy loss. Therefore, numerical simulation of the whole debris flow movement process during the outburst time can be carried out under complex terrain conditions. This is of great significance to the safety of engineering construction and disaster prevention.

This study was conducted on several debris flows in the reservoir area of the pumped storage power station in Shangyi County, Hebei Province. The on-site investigation showed that many gullies in the study area are filled with large-scale slag debris from a mining project. The possibility of debris flow is very high. Therefore, a detailed assessment of geological conditions, such as topography and source distribution, combined with indoor analysis and experimentation, led to multiple evaluation factors being selected for use in the neural network algorithm, which was employed to carry out risk assessment and zoning of the study area. Then, a shallow-water model (SWM) based on the finite volume method (FVM) was used to simulate and forecast the debris flow's scale and hazard range for the high-risk gullies based on rainfall frequencies of 20, 50, 100, and 200 years. Finally, the sensitivity of parameters affecting debris flow migration is analyzed, and the results were compared with the results calculated by the Flo-2D software. Some theory and advantages underlying the finite volume shallow water flow model were discussed.

Study area

Topography and structural conditions

The study area is located in Xiaosuangou, Shangyi County, Hebei Province (Fig. 1a), which belongs to the northern Hebei mountain area in the southern part of the Yinshan mountain range (Fig. 1b, c).

The terrain of the project area changes greatly, which is manifested as high topography on the east and west sides and low topography in the middle. The elevation generally varies from 873 to 1600 m. In the vicinity of the ridge, the bedrock cliffs are exposed and the slope is generally above 45°. The terrain is relatively flat near the valley (Fig. 2). The geomorphologic type is classified as an erosion mountain and mainly manifests as a medium and low mountain region. In addition, the surface elevation of the Dongyang River flowing through the study area changes from 950 to 910 m. The elevation and width of the riverbed are 880~900 m and 10~20 m, respectively. In general, the Dongyang River's left bank topography is steeper than that of the right bank.

There are nine large gullies in the study area—Dong, Shaliangquan, Qinghutai, Pingantai, Hou, Nan, Dahu, Xiaohu, and Caonian gullies (Fig. 3a). The gully terrain changes from high and steep in the upstream to low and gentle in the downstream (Fig. 3b). The cross section is V-shaped (Fig. 3c). There are alluvial-diluvial deposits and artificially accumulated slag bodies in the gullies. The larger waste slag bodies are mostly distributed in a platform shape (Fig. 3e), and are mainly concentrated in the middle and lower reaches of the gullies, which changed the gullies' local terrain. In addition, the study area has two

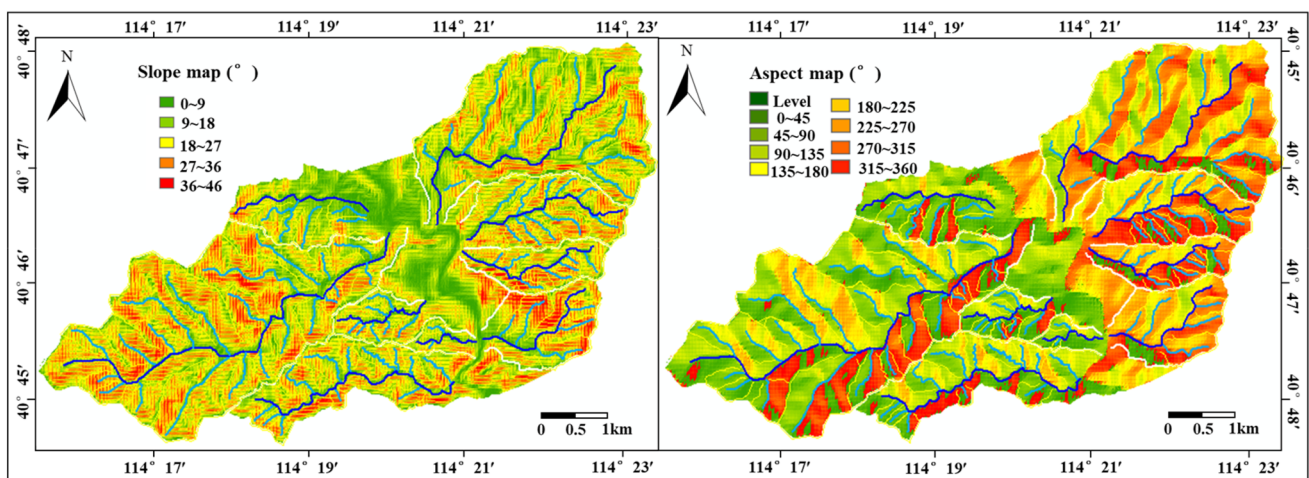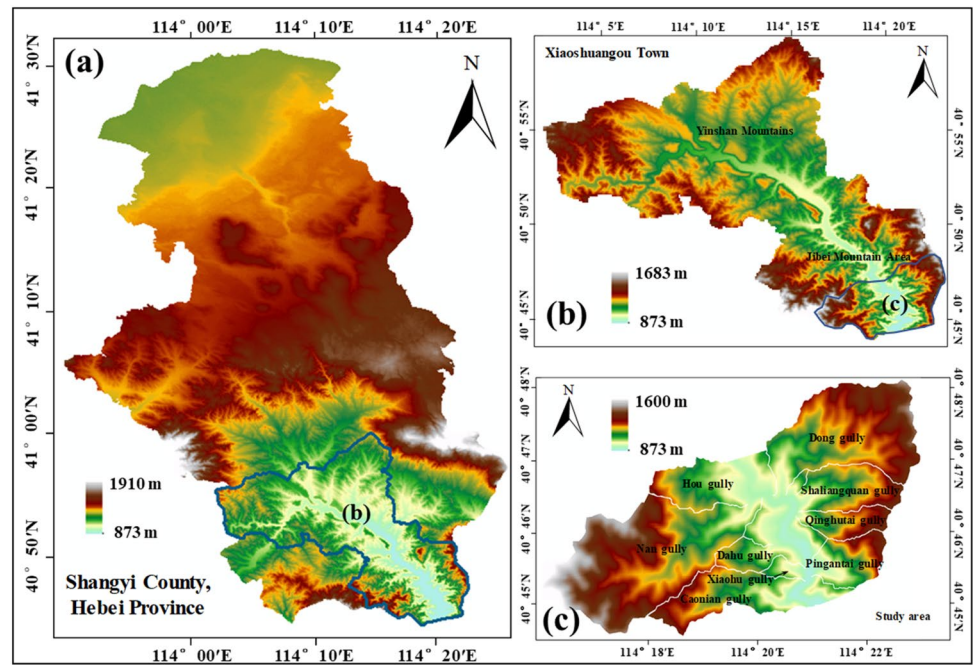**Fig. 1** The location and terrain of the study area

Fig. 2 Slope and aspect map of the study area

levels of river terraces (Fig. 3d). The height of terrace I is 5~10 m, and the height of terrace II is 15–20 m.

The study area is located in the secondary geotectonic unit of the North China Platform. The exposed lithology is mainly Archean gneiss, granulite, Proterozoic metamorphic monzonitic granite, and Jurassic conglomerate, sandstone (Fig. 4). The Quaternary lithology is mainly distributed in the Huai'an Basin in the southern part of the study area. In addition, there are two NW–SE normal faults in the study area, which intersect with the Dongyang River at a small angle. The site's basic seismic intensity in the project area is VII, indicating site with poor regional structural stability.

Rainfall conditions

The study area is a cold, temperate continental monsoon climate with four distinct seasons, cold and dry winters and has less winds in spring and autumn, less rain in summer. Based on the Shangyi Weather Station statistics from 1960 to 2014, the maximum (1978) and minimum (1962) annual precipitation were 646.9 mm and 217.9 mm, respectively, while the average annual precipitation was 414.0 mm. Precipitation is unevenly distributed during the year and is mainly concentrated in the summer. 77.2% of the annual precipitation occurs between June and September, while only 5.0% occurs from November to March (Fig. 5).

Fig. 3 Terrain condition. **a** Relative position and topography of each gully. **b** Highest point in the study area. **c** V-shaped valley. **d** River terraces. **e** Waste slag body in Nan gully
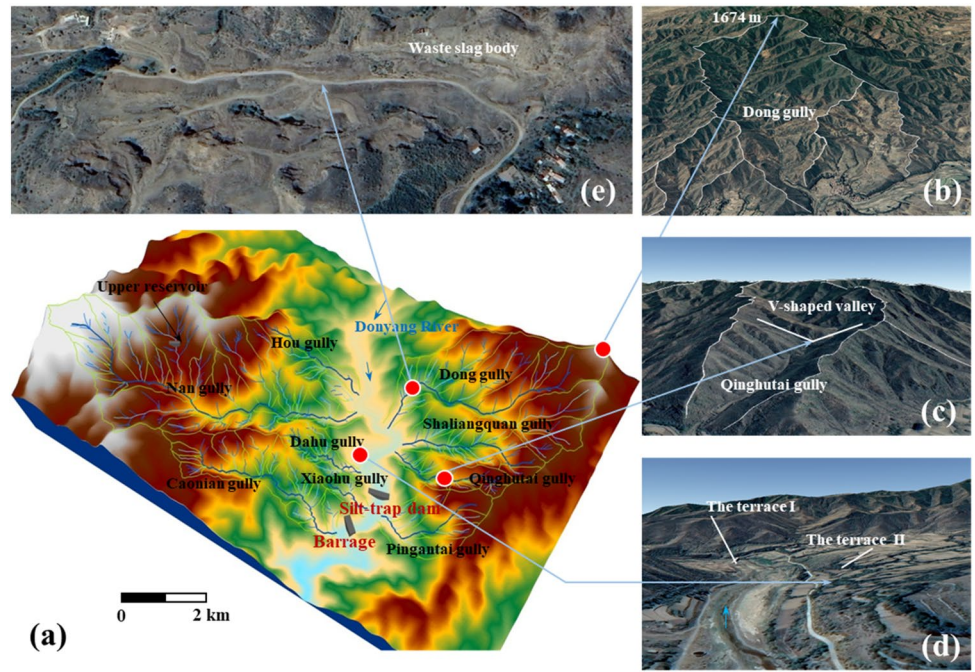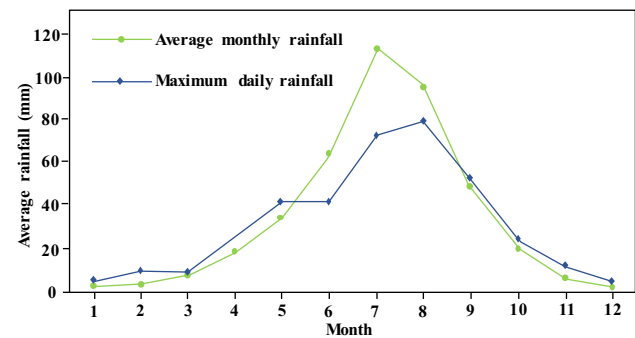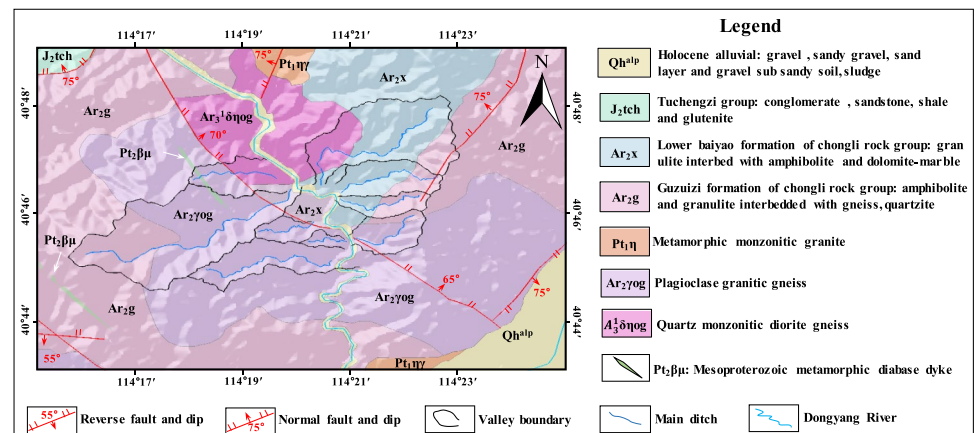

Fig. 4 Geological map of the study area

Fig. 5 The average monthly rainfall and maximum daily rainfall of Shangyi County

Table 1 Rain intensity statistics provided by Chaigaobao rainfall station

Maximum rainfall intensity		Occurrence time
10 min	24.5 mm	1973.6.19
1 h	64.9 mm	1994.7.20
6 h	124.5 mm	1994.7.20
1 day	124.6 mm	1994.7.20

The rainfall characteristics shown in Table 1 were obtained using the measured rainstorm data statistics from 1956 to 2016 provided by Chaigoubao hydrology station.

Engineering geological condition

Currently, plans are to establish a pumped storage power station in the study area to alleviate the power shortage issues in Hebei (Fig. 6a). The power station pivot project's main buildings are composed of an upper reservoir, a lower reservoir, a waterway system, and an underground powerhouse system. The upper reservoir is intended to be built on the left bank tributary in the upper reaches of Nan gully. The waterway system is arranged in the mountain ridge between Nangou and the Dongyang River. Construction of the lower reservoir is scheduled to take place at the Caonian gully mouth, and installation of a silt-trap dam is planned on the downstream side of the Dahu gully mouth. The project area's terrain is conducive to catchment, so the risk of flooding and debris flows is amplified (Fig. 6b–e).

The vegetation coverage in the study area is low (Fig. 7a). Anthropogenic activities, and specifically extensive mining, have caused major changes to the gullies' natural environment. In recent decades, Dong, Shaliangquan, Pingantai, Hou and Nan gullies have produced large-scale waste slag bodies. These waste slag bodies with no solidification and no reinforcement measures are scattered throughout the area (Fig. 7b). Obvious tensile cracks have been found on

the surface of some accumulation platforms (Fig. 7c, d). In addition, the bedrock joint fissures exposed in the study area are relatively developed (Fig. 7e, f). The surface rock mass is broken due to weathering, unloading, and artificial excavation. New collapses and landslides can be seen on both sides of the gully (Fig. 7g, h). These loose deposits are an important source for debris flows. Furthermore, observation of debris-flow deposits (Fig. 7i, j) indicates that such events have historically occurred in the study area. Thus, debris flows may pose a threat to the storage power station. The analysis and forecasting of the risk and hazard range associated with the nine debris flow gullies are of critical importance.

Risk assessment

The risk assessment is used to determine the probability of debris flow in each gully, so as to provide the basis for the implementation of numerical simulation. Risk assessment should be based on site surveys. However, the influence of human error is difficult to eliminate, and similar data values are easily classified into different levels during the evaluation process. In order to reduce the influence of fuzzy
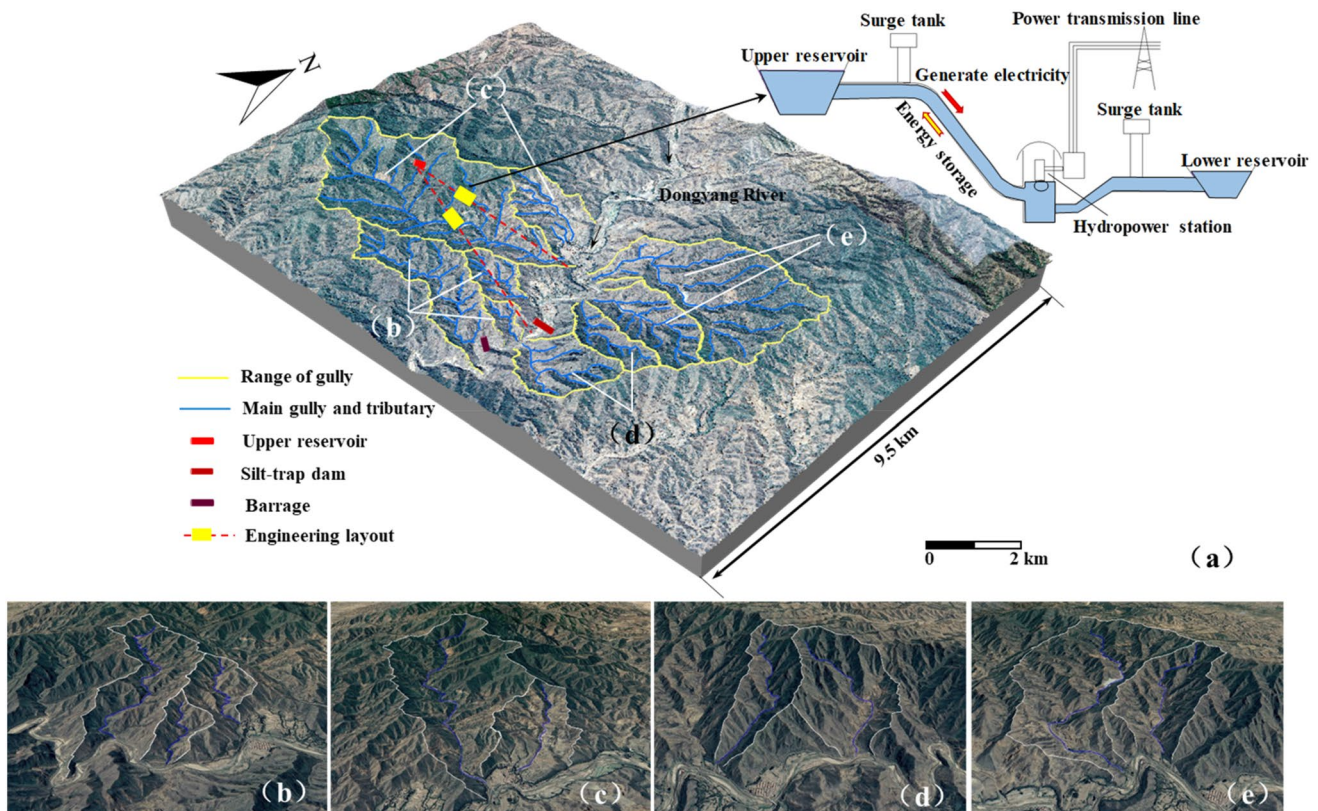

Fig. 6 Image maps. **a** 3D image map of the study area. **b** Caonian, Dahu, and Xiaohu gullies. **c** Nan and Hou gullies. **d** Qinghutai and Pingantai gullies. **e** Dong and Shaliangquan gullies

Fig. 7 Site investigation. **a** Vegetation conditions. **b** Large waste slag accumulation platforms in the study area. **c** and **d** Waste slag bodies that produce deformation and cracks. **e** Layered rock mass. **f** Broken rock mass with high degree of weathering. **g** Landslide. **h** Colluvium. **i** Debris flow accumulation in Pingantai gully. **j** Partial photo of debris flow

discriminant, a neural network model was adopted so that multiple factors are selected to comprehensively evaluate the risk of each gully.

The evaluation unit

Due to the small size of the study area, each gully and the corresponding branch ditch were selected as the evaluation units. The evaluation units were obtained by hydrological analysis with GIS software. The study area was divided into 117 small basin units, of which 72 are larger in area and depict more obvious valley form. The other 45 basin units are small and some are in the early stages of development.

Evaluation factor

Impact factor

The risk of a debris flow needs to be comprehensively determined by various impact factors. It is important to designate major and secondary factors from multiple potential factors. As such, 11 risk assessment factors were selected using the "Debris Flow Risk Assessment" method

(Liu et al. 1995) in conjunction with actual site investigation. The main influencing factors were L_1 (Maximum amount of debris flows per 100-years return period) and L_2 (Debris flow frequency); S_1 (basin area), S_2 (main gully length), S_3 (maximum relative height difference), S_4 (cutting density), S_5 (bending coefficient), S_6 (Mud and sand recharge section length ratio), S_7 (Solid loose material per unit area), S_8 (daily maximum precipitation) and S_9 (the population density) were secondary factors. The specific definitions for all factors are as follows:

1. Basin area S_1 (km^2): catchment area of debris flow. The larger the area, the greater the amount of catchment.
2. The length of the main gully S_2 (km): the length from the gully source along the main gully to the gully mouth.
3. Maximum relative height difference S_3 (m): the elevation difference between the basin's highest point and the gully mouth. It reflects the debris flow's potential energy.
4. Cutting density S_4 (1/km): the ratio of the watershed's relative height difference to the length of the main gully.

5. Bending coefficient S_5: the ratio of the gully's actual length to the straight-line length.
6. Mud and sand recharge section length ratio S_6: the ratio of the section length that can recharge the debris flow to the gully's total length.
7. Solid loose material per unit area S_7 (10^4 m^3/km^2): the ratio of the total solid loose material reserve to the catchment area. This factor reflects the potential scale of the gully's debris flow. Because this factor varies greatly among different basin units, the following quantitative indicators were employed (Table 2).
8. Daily maximum rainfall S_8 (mm): the maximum amount of rainfall throughout the day. This is the direct factor that triggers debris flows.
9. Population density S_9: reflects, to some extent, the potential impact of human activities on debris flow incidents.
10. The maximum outflow of debris flow L_1 (10^4 m^3): the maximum outflow of debris flow during a 100-year rainfall frequency. This factor is a direct assessment of the debris flow intensity, which is mainly determined through field surveys and indoor calculations.
11. Debris flow occurrence frequency L_2 (times/100 years): the number of debris flow occurrences per unit time.

Among the above impact factors, attribute value extraction of the geological parameters for each evaluation unit is mainly realized by the ArcGIS platform's spatial analysis function. The L_1, L_2, and S_6–S_{10} factors are determined based on field investigations combined with indoor calculations. Table 3 lists the impact factor parameter values of each main gully's watershed unit. Because there are so many branch ditch watershed units, they were omitted from Table 3.

Table 2 S_7 factor quantization table

S_7 (10^4 m^3/km^2)	> 10	5~10	5~1	< 1
Quantitative indicators	4	3	2	1

Disaster source point

Disaster source points are determined by means of field investigation based on the unique geological condition because the waste slag bodies are distributed throughout the study area. Debris flow activities are found in the disaster source points, which are represented by erosion, deformation and sliding in different degrees. Moreover, the disaster source point distribution is largely related to the size and location of the waste slag bodies (Fig. 8). The disaster source points with impact factor attribute values are used as the target factor and are calculated by the model at a later time, with a mark of 1. Non-disaster source points are randomly generated in the study area, with a mark of 0.
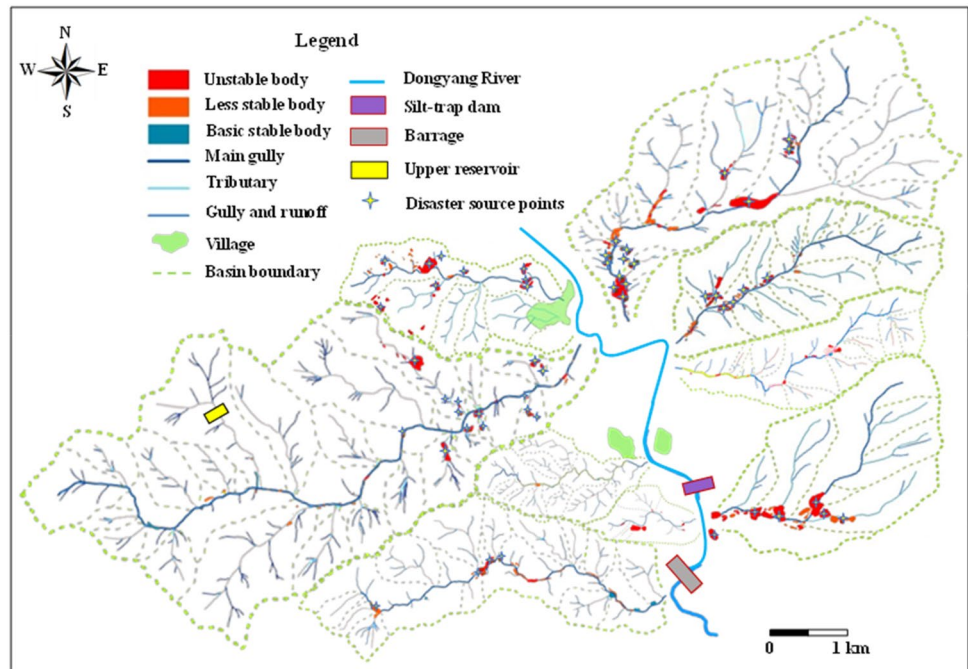
Occurrence probability of debris flow

Artificial neural network is an abstract mathematical model that addresses problems by simulating human brain neurons. The method has strong self-learning and adaptive ability (Han et al. 1996; Chang et al. 2007). There are numerous types of impact factors and risk classifications associated with a comprehensive evaluation of debris-flow risk. Therefore, each impact factor of the same basin unit may fall into a different risk interval. As a result, it is more difficult to determine the degree of risk. Because the neural network is highly capable of dealing with non-linear problems that exhibit unclear relationships between conditions and targets, this model was selected to predict the probability of debris flow.

Neural network model

The three layers BP neural network model (input layer, hidden layer, and output layer) based on multi-layer perceptron (MLP) was trained in this work. A highly non-linear mapping relationship between the input and output layers is adaptively obtained through learning. Assuming that the input layer was $X = (x_1, x_2, x_3 \ldots x_n)$; and the output layer was $Y = (y_1, y_2, y_3 \ldots y_n)$. The number of hidden

Table 3 Watershed characteristic parameters

Gully	S_1 (km^2)	S_2 (km)	S_3 (m)	S_4 (1/km)	S_5	S_6	S_7	S_8 (mm)	S_9	L_1 (10^4m^3)	L_2
Dong	7.389	5.670	542	4.056	1.29	0.4	4	125	0	8.84	0
Shalianquan	2.713	3.103	471	5.29	1.13	0.3	3	125	0	3.98	0
Qinghutai	1.397	2.832	459	6.68	1.16	0.25	1	125	0	0.92	0
Pingantai	1.976	2.438	484	4.296	1.24	0.6	4	125	0	2.73	0
Hou	2.054	2.945	394	5.90	1.186	0.6	4	125	0	3.3	0
Nan	11.108	7.587	773	4.78	1.22	0.3	3	125	0	4.43	0
Dahu	1.081	2.349	308	9.15	1.30	0.09	1	125	0	0.77	0
Xiaohu	0.418	1.327	222	6.62	1.205	0.5	1	125	0	0.34	0
Caonian	3.221	3.926	484	5.78	1.18	0.2	2	125	0	1.71	0

Fig. 8 The material source distribution map of the study area

layer neurons is n. W_{ij}, W_{jk} ($W_{ij} \in R^{n \times s}$, $W_{jk} \in R^{s \times 3}$) are the association weight matrices between the input layer and the hidden layer and the output layer and the hidden layer, respectively. The w_{ij} and w_{jk} are corresponding association weights. R is a space concept. Θ_j, Θ_k ($\Theta_j \in R^s$, $\Theta_k \in R^3$) are the threshold vectors between the input layer and the hidden layer, and the output layer and the hidden layer, respectively. θ_j and θ_k are corresponding thresholds. The correlation between the above parameters constitutes a non-linear mapping from the input space R^n to the output space R^3. Z_p is the hidden layer's output vector. Thus, the relationship among the input, hidden, and output layers can be expressed by the following formula (Wang et al. 2003):

$$Z_p = f\left(w_{ij} \times x_p + \theta_j\right), \tag{1}$$

$$y_p = f\left(w_{jk} \times Z_p + \theta_k\right), \tag{2}$$

where, x_p is the input vector, y_p is the output vector, and f is the nonlinear activation function that can be expressed as a Sigmoid Function:

$$f(\mu) = \frac{1}{1 + e - \mu}. \tag{3}$$

The minimum root mean square (RMS) error obtained by the gradient descent method was used to demonstrate successful completion of the training.

$$\text{RMS} = \sqrt{\frac{1}{2} \sum_{p=1}^{N} \left(y_p - d_p\right) 2} = \min(\text{RMS}), \tag{4}$$

where N is the number of training samples and d_p is the expected output value. RMS can be minimized by setting training times, training cycles, and achieving target accuracy.

Model building and training

The neural network model was constructed based on the above principles. The 11 impact factors were used as the input layer (Fig. 9), and the disaster source points were used as the target factor for model training. The maximum training time was set to 15 min and the overfitting limit was 30%. After modeling was complete, a uniform point cloud with a spacing of 20 m was generated throughout the study area, and the corresponding impact factor attribute field values were extracted. Then, these field values were used to import the foregoing obtained neural network model and calculate the probability value of debris flow occurrence at each point. Finally, the weighted prediction values (Fig. 10a) of each impact factor were obtained. Due to S_9 and L_2 both being 0, these two impact factors were eliminated. The weights of L_1, S_7, and S_6 were largest, followed by S_2, S_4, S_1, S_5, and S_8. The S_3 was of low importance. The probability value of debris flow in each
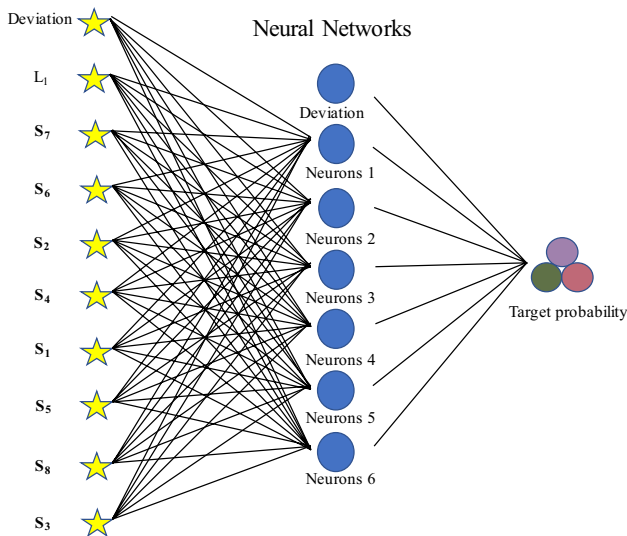
Fig. 9 The neural networks

Table 4 Risk classification table

Levels of risk	Very low	Low	Moderate	High	Very high
Occurrence probability	0.02~0.16	0.16~0.33	0.33~0.52	0.52~0.71	0.71~0.90

Risk zoning

The natural discontinuity method was used to classify the probability values of debris flows that may occur in each basin unit of the study area (Table 4). The corresponding risk partition map was generated (Fig. 11) according to Table 4.

The results show that there is a high risk of debris flows in the upstream and left bank of the Hou gully and downstream of Nan gully. The risk is also high in the downstream of Dong and Shaliangquan gullies. The risk in the middle and lower reaches of Pingantai gully is medium–high. The results of the other debris flow risk assessment were low or very low.

Further analysis found that the L_1, S_6, and S_7 were also larger in the high-risk basins. Therefore, these three factors greatly affect the risk level. In addition, there was obvious erosion and silting-up in high-risk basins; and the waste slag bodies were deformed and showed local collapse. Therefore, the evaluation results were reasonable and consistent with the qualitative interpretation of the field survey.

basin unit was between 0 and 0.9. The accuracy of the neural network model can be evaluated by receiver operating characteristic curve (ROC) (Sun et al. 2018, 2020). The ROC curve is a sensitivity (ordinate) and specificity (abscissa) relationship curve based on multiple different thresholds (impact factors). The area under the ROC curve (AUC) is used to quantitatively evaluate the accuracy of the neural network model. The closer the AUC is to 1, the higher the prediction accuracy of the model. In this study, based on the results of the neural network model, random points are generated in the debris flow and non-debris flow areas. Then the influencing factor attribute value is extracted to the points and the ROC curve analysis is performed (Fig. 10b). The value of AUC is 0.862, the model accuracy is good (Sun et al. 2018, 2020).

Numerical simulation

According to the result of the risk assessment, SFLOW software was used to predict the hazard range of 5 high-risk debris flow gullies.

Fig. 10 **a** Histogram of each influence factor weight. **b** The ROC curve of neural network model

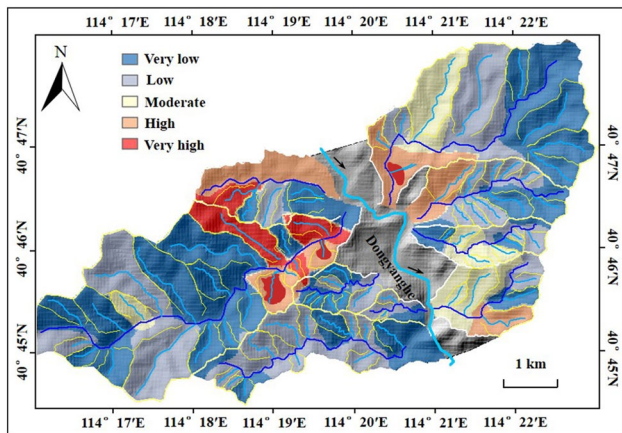**Fig. 11** Zoning map of risk assessment results in the study area

Numerical model

In the numerical model, SFLOW uses a finite volume method based on the Godunov format to solve the shallow water flow equation. By assuming that the fluid's vertical direction satisfies the hydrostatic pressure and velocity uniformity, the Navier–Stokes equation can be simplified to the following form (Ouyang et al. 2013):

$$\frac{\partial q}{\partial t} + \frac{\partial f}{\partial x} + \frac{\partial g}{\partial y} = s,$$ (5)

$$q = \begin{bmatrix} h \\ q_x \\ q_y \end{bmatrix} = \begin{bmatrix} h \\ uh \\ vh \end{bmatrix},$$ (6)

$$f = \begin{bmatrix} uh \\ u^2h + \frac{1}{2}gh^2 \\ uvh \end{bmatrix},$$ (7)

$$g = \begin{bmatrix} vh \\ uvh \\ v^2h + \frac{1}{2}gh^2 \end{bmatrix},$$ (8)

$$s = \begin{bmatrix} 0 \\ -gh\frac{\partial z_b}{\partial x} - S_{fx} \\ -gh\frac{\partial z_b}{\partial y} - S_{fy} \end{bmatrix},$$ (9)

where: h is the water depth; Z_b is the bed's altitude; g is the gravitational acceleration; $q_x(= uh)$ and $q_y(= vh)$ represent the single-width flow in the x-direction and the y-direction, respectively; and S_{fx} and S_{fy} represent the frictional resistance in the x- and y-directions, respectively.

The rheological friction model incorporates the debris flow fluid's friction properties, viscosity properties, and solid particles' contact energy loss. The model is mathematically expressed as follows (Zhang et al. 2015):

$$S_{fy} = \frac{\tau}{\rho_m} + \frac{K\eta v}{8\rho_m h} + \frac{gn_{td}^2 v^2}{h^{1/3}},$$ (10)

$$S_{fx} = \frac{\tau}{\rho_m} + \frac{K\eta u}{8\rho_m h} + \frac{gn_{td}^2 u^2}{h^{1/3}},$$ (11)

where τ is the yield stress (Pa); ρ_m is the density of solid matter in the debris flow (kg/m^3); K is the drag coefficient; η is the fluid viscosity (Pa s); and n_{td} is the equivalent Manning coefficient. The yield stress and fluid viscosity are defined as:

$$\tau = \alpha_2 \exp\left(\beta_2 \cdot C_v\right),$$ (12)

$$\eta = \alpha_1 \exp\left(\beta_1 \cdot C_v\right),$$ (13)

where α_1, α_2, β_1, and β_2 are empirical parameters and C_v is the sediment volume density.

Data preprocessing

The SFLOW software needs to confirm terrain, inflow point, hydrology, and rheological parameters. The terrain parameters in ASCII code were obtained from a 7.24 m × 7.24 m Digital Elevation Model (DEM). When simulating the debris flow, it is necessary to specify the inflow point of the debris flow in advance. According to the risk assessment results (Fig. 11), the inflow points should be downstream from a large number of waste slag bodies and the gullies with a higher degree of risk.

The rheological parameters reflect the deformation and flow properties of the debris flow, which is related to the viscosity. Particle analysis experiments can be used to determine particle size (Yu et al. 2020; Zhang et al. 2020). The experimental curve shows that the waste slag and the early debris flow accumulation in the gully (Figs. 12, 13) are mainly medium-grained soil. The clay (< 0.005 mm) content is almost 0. Therefore, the debris flow can be considered of low viscosity (Ni et al. 2011). Based on the field investigation combined with the technical standard "Specification of geological investigation for debris flow stabilization (DZ/T0220-2006) (2006)," the debris flow density of each gully is shown in Table 5.

The rheological parameters α_1, α_2, β_1, and β_2 were determined by previous experiments (Lin et al. 2005; O'Brien 2006) and some of the typical debris flow events (Chen et al. 2018; Chang et al. 2017; Han et al. 2017, 2018; Bao et al.
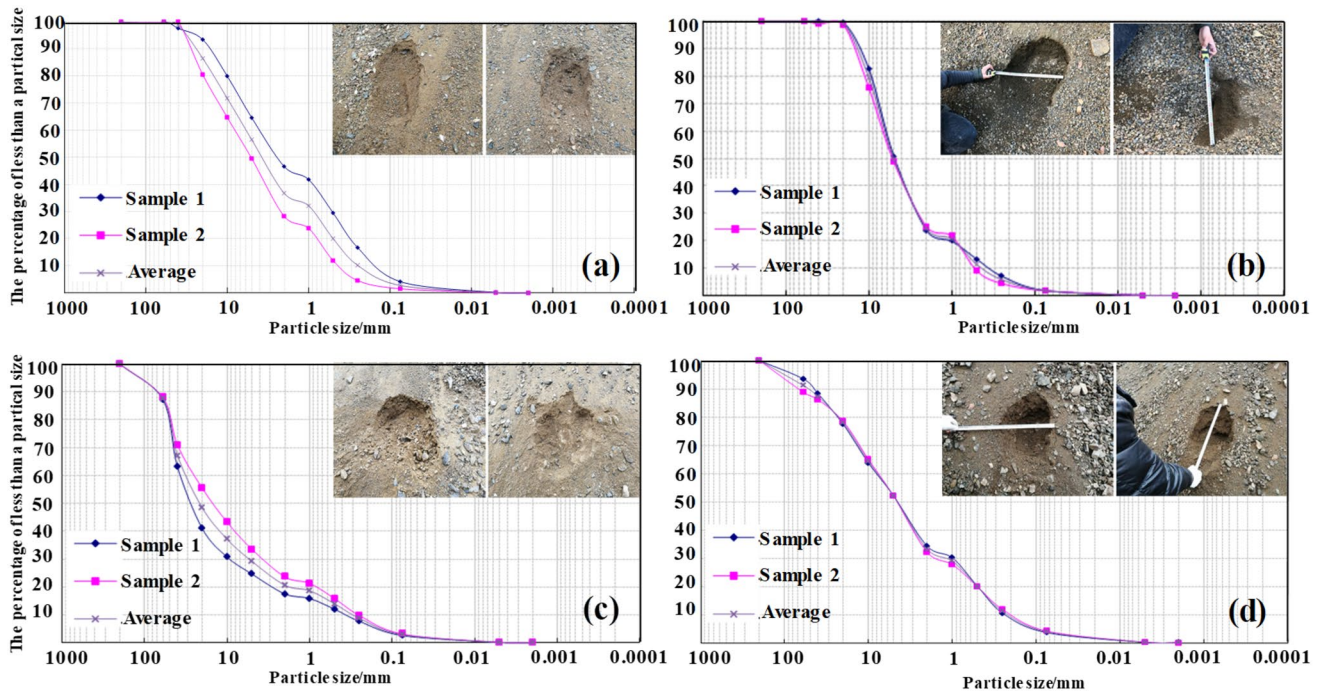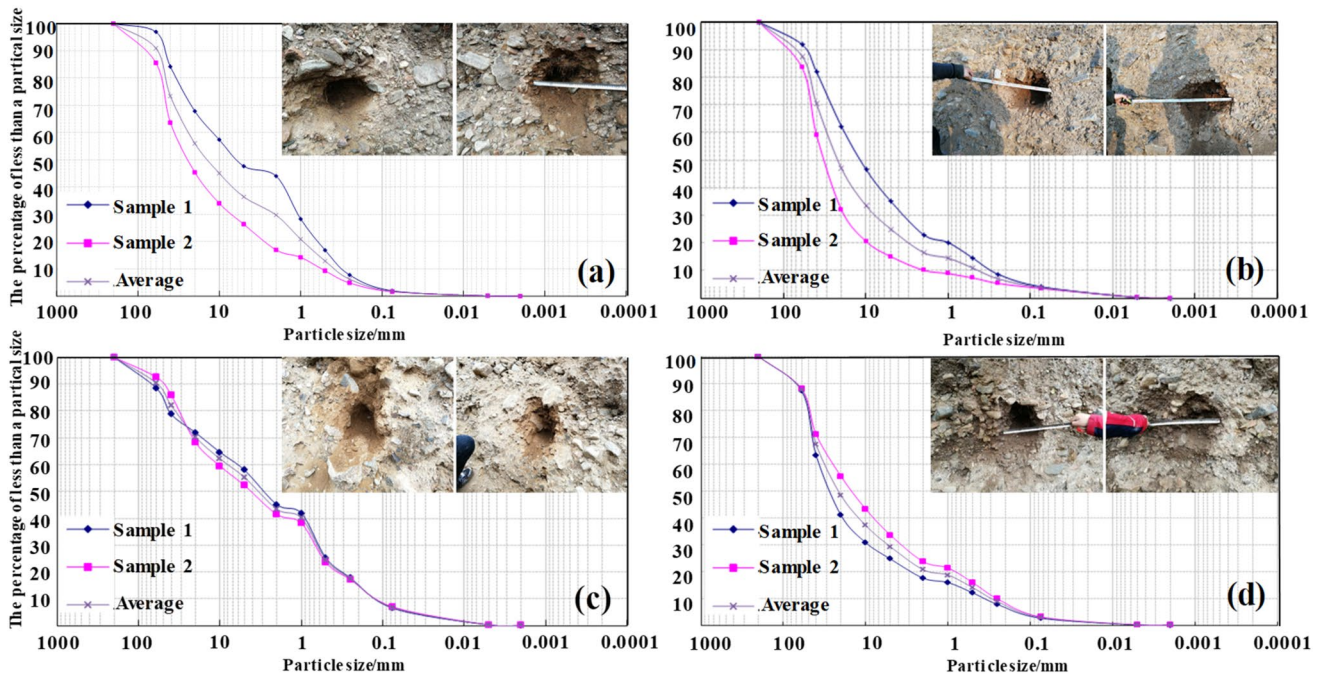
Fig. 12 Particle size distribution curve of waste slag

Fig. 13 Particle size distribution curve of debris flow

Table 5 Debris flow density of each gully

Gully	Dong	Shaliangquan	Pingantai	Hou	Nan
Density (kg/m³)	1600	1502	1586	1572	1544

2019a, b). The C_v parameters calculated by formula 14–17 are 0.4 (Dong), 0.336 (Shaliangquan), 0.391 (Pingantai), 0.381 (Hou), and 0.363 (Nan), when the density of water (ρ_w) is 1000 kg/m³, the mixture density (ρ_m) is 2500 kg/m³.

$$C_v = \frac{V_s}{V_s + V_w}, \tag{14}$$

$$\rho_n = \frac{(d_s f + 1)\rho_w}{f + 1}, \tag{15}$$

$$f = \frac{V_s}{V_w}, \tag{16}$$

$$d_s = \frac{\rho_m}{\rho_w}, \tag{17}$$

where, ρ_n is the debris flow density (kg/m³); ρ_w is the density of water (kg/m³); ρ_m is the sediment mixture density (kg/m³); d_s is the relative density of the solid particles; and f is the ratio of solid material volume V_s to water volume V_w. The laminar flow retardation coefficient K and Manning coefficient n related to the surface condition are selected as 2500 and 0.13 (Han et al. 2017, 2018; Chen et al. 2018; Bao et al. 2019b). Finally, all rheological parameters are shown in Table 6.

The hydrological parameters are mainly the flow and duration of the debris flow process curve. The flood peak flow can be calculated by the rain flood method, expressed as follows:

$$Q_p = \overline{C}K_p F^n, \tag{18}$$

where Q_p is the flood peak flow at design frequency (m³/s); $\overline{C}$ is the multi-year average peak flow modulus coefficient ($\overline{C} = 8$); K_p is the modulus coefficient at the same frequency as the flood peak flow (when the deviation coefficient

$C_s = 3.5C_v$ and the local area's variation coefficient $C_v = 1.0$, then the K_p can be obtained by the Pearson type III K_p value); F is the basin area (km²); and n is the basin area index ($n = 0.67$ when $F < 30$ km²). The total flood volume and peak duration are determined by the following two equations:

$$V_p = 0.1HF, \tag{19}$$

$$T_p = 0.278(V_p/Q_p), \tag{20}$$

where H is the gully runoff depth (cm); Then the debris flow peak flow can be expressed as:

$$Q_c = (1 + \varphi)Q_p D_c, \tag{21}$$

where Q_c is the debris flow peak flow (m³/s); $1 + \varphi$ is the correction coefficient; and D_c is the blockage coefficient. φ and D_c were selected in conjunction with the "Specification of geological investigation for debris flow stabilization (DZ/T0220-2006)." Considering that the solid matter in the debris flow has a significant amplification effect on the flooding time, the expansion coefficient BF was used to determine the debris flow duration (BF = $1/C_v$). Finally, the debris flow simulation calculation parameters are shown in Table 7 and the hydrographs for the 20, 50, 100, and 200-year return periods are presented in Fig. 14.

Results

Figure 15 shows the movement path, accumulation range, and thickness of each debris flow at the different return periods. The debris flow range and thickness are larger in Nan and Dong gullies. The debris flow depth in Nan gully ranges from 7 ~ 8.2 m, while that in Dong gully is from 6.1 to 7.2 m. In the remaining valleys, the flow depth is mostly distributed at 4 ~ 5 m. The simulated debris flow thickness is generally similar to the field survey. In addition, once the debris flow breaks out, the area near the flow path will be affected on the order of hundreds of meters or possibly even a few kilometers. In terms of scale, Nan gully has the largest impact area of 163,836 m² and a migration distance of 1511 m. Dong gully is second, with a maximum impact area

Table 6 Empirical parameters in numerical simulation

Parameters	Units	Values	Remarks
α_1	0.1 Pa s	0.6488	For viscosity
β_1	–	13.72	For viscosity
α_2	kPa	0.00462	For yield stress
β_2	–	11.24	For yield stress
K	–	2500	Resistance coefficient
n	–	0.13	Manning coefficient

Table 7 The parameters and the duration of debris flow in the numerical simulation

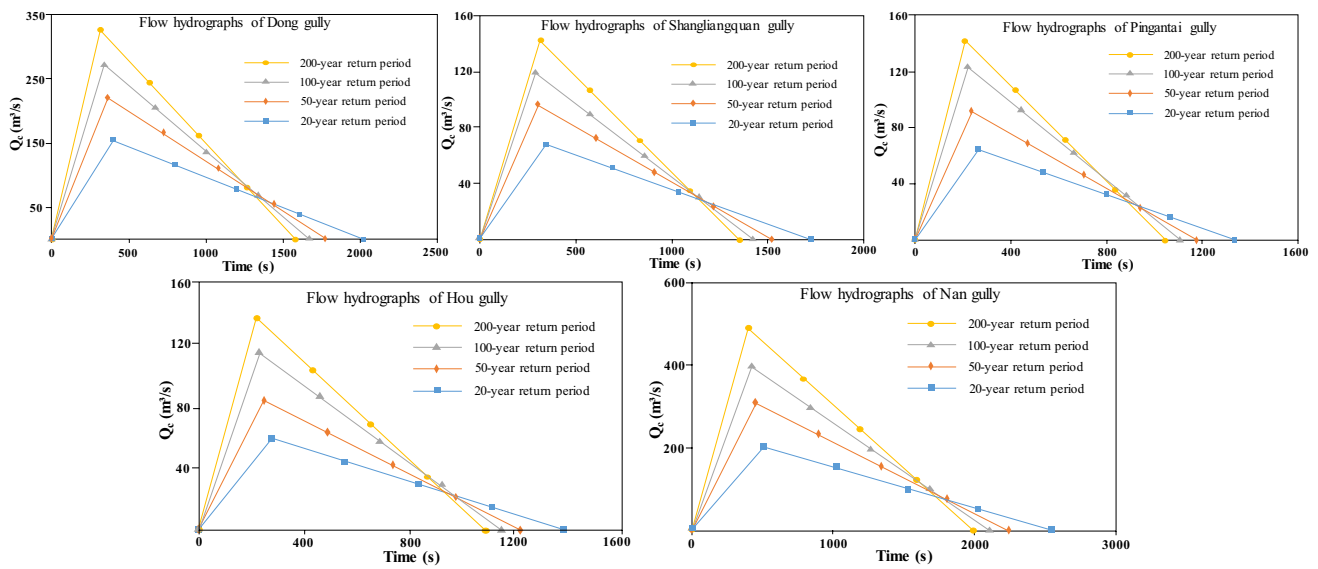| Gully	ρ_m(kg/m³)	τ (Pa)	η (Pa s)	K	n	T (s)
Dong	2500	414.2	156.9	2500	0.13	2017/1777/1669/1577
Shaliangquan	2500	201.8	65.2	2500	0.13	1725/1520/1428/1349
Pingantai	2500	374.4	138.6	2500	0.13	1335/1176/1105/1044
Hou	2500	334.6	120.9	2500	0.13	1388/1223/1149/1085
Nan	2500	273.3	94.4	2500	0.13	2542/2239/2104/1988

Fig. 14 Flow hydrographs used in the simulation

Fig. 15 Run-out result prediction of flow path and depth of potential debris flow. **a** 20-year return period. **b** 50-year return period. **c** 100-year return period. **d** 200-year return period
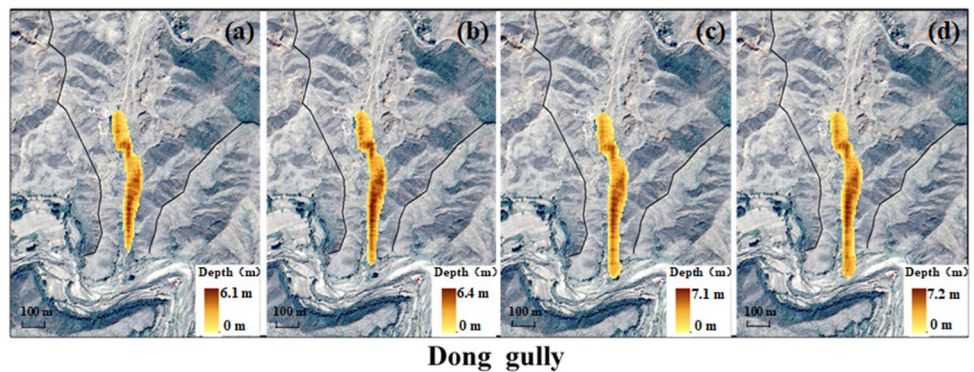
of 71,680 m², and a migration distance of 930 m. Due to the limited area of catchment and source volume, the remaining gullies have a smaller accumulation range— mainly ranging from 39,728 ~ 46,554m²; and a stacking length from 400 to 564 m.

To further explain the relationship between the debris flow scale and different rainfall frequencies in each gully, the relationship between the simulation variables (transport distance, stacking thickness, and affected area) and the rainfall frequency is demonstrated in Fig. 16. Each simulation variable has a nonlinear relationship with rainfall frequency— lower rainfall frequency corresponds to a larger scale of debris flow outbreak, impact range, and accumulation thickness. Therefore, the lower the frequency, the greater the risk.

The debris flow evaluation results using different rainfall frequencies were combined with the reservoir area image during normal water storage (Fig. 17). It can be found that the debris flow into the reservoir area increases gradually with the decrease of frequency. When the return period is

200 years, the total volume of debris flows into the reservoir will reach 45,894 m³ (Fig. 18). This will raise the reservoir area's water level of 81,8471 m² by less than 0.1 m. However, the normal water level is more than 20 m from the top of the dam according to the design. Therefore, the debris flows will not pose an enormous threat to the reservoir area.

Discussion

In the simulation of debris flow, the selection of rheological parameters is very important. τ, η, K, and n in rheological parameters play a decisive role in the migration of debris flow (Bao et al. 2019b; Chen et al. 2013). However, once the site conditions and material composition are determined, α_1, α_2, β_1, β_2, and K can basically be determined. Therefore, the main parameters affecting the migration of debris flow are the volume concentration C_v of debris flow (formula 12, 13) and Manning coefficient n (surface roughness of gully).

Fig. 15 (continued)

Shaliangquan gully

Pingantai gully

Hou gully

Nan gully
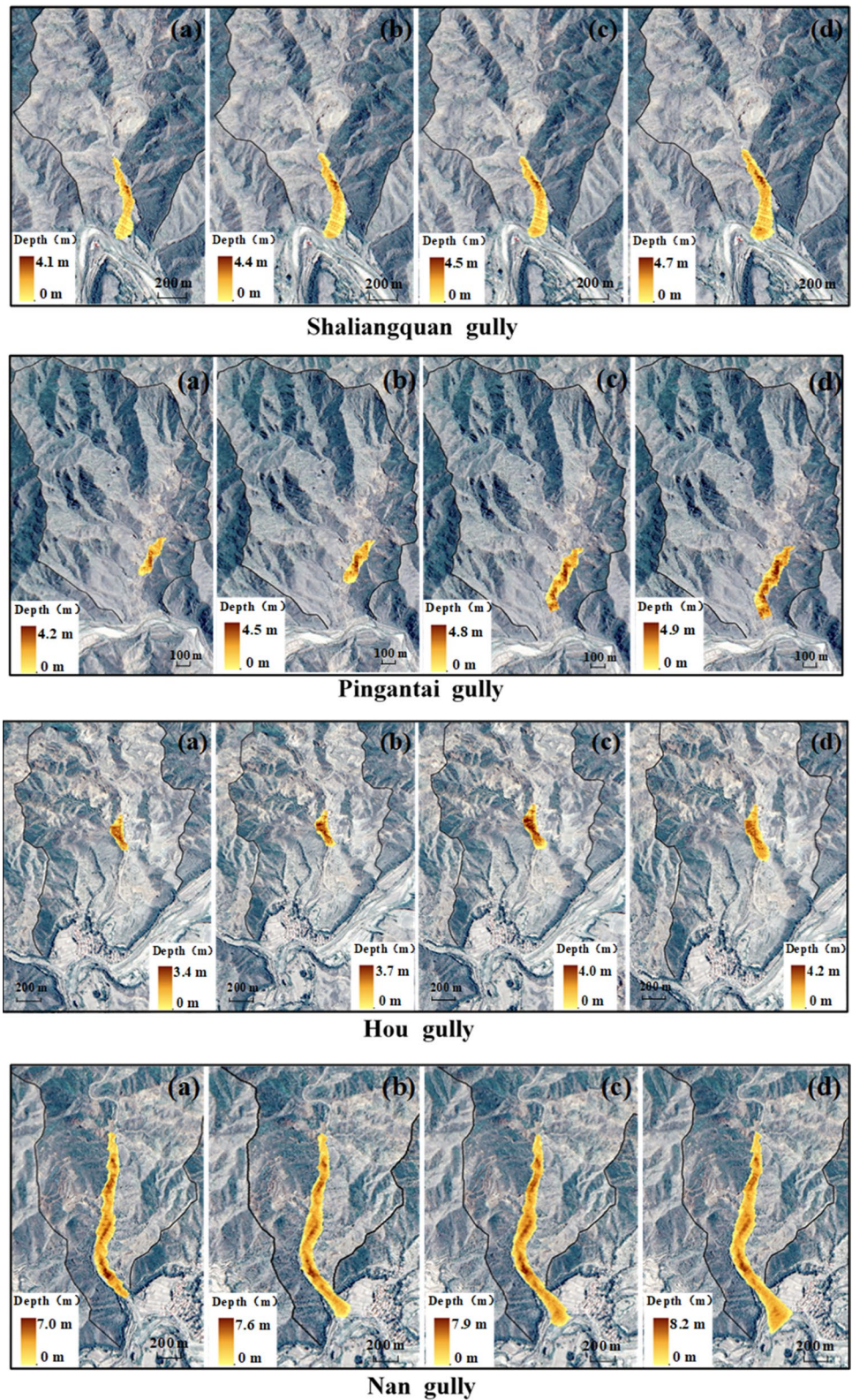
To further analyze the effects of these two parameters, taking Dong gully in 200-year return period as an example, the influence of different C_v and n values on the simulation results is analyzed. The two parameters are set to three levels: low, medium and high (Bao et al. 2019b; O'Brien 2006), and the corresponding values are shown in Table 8. The
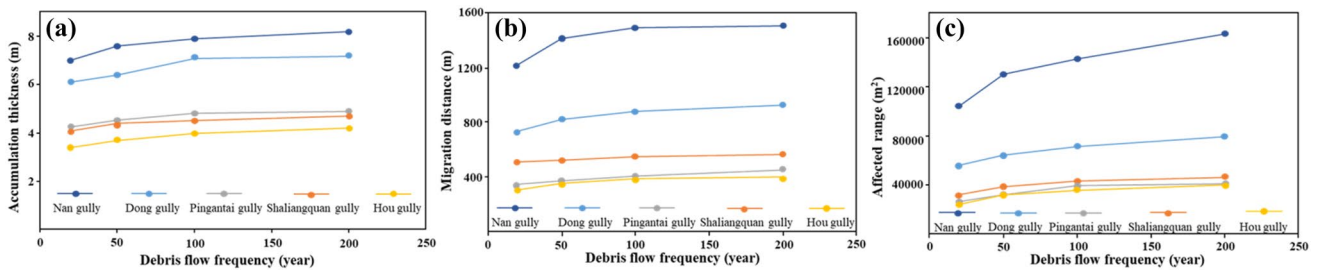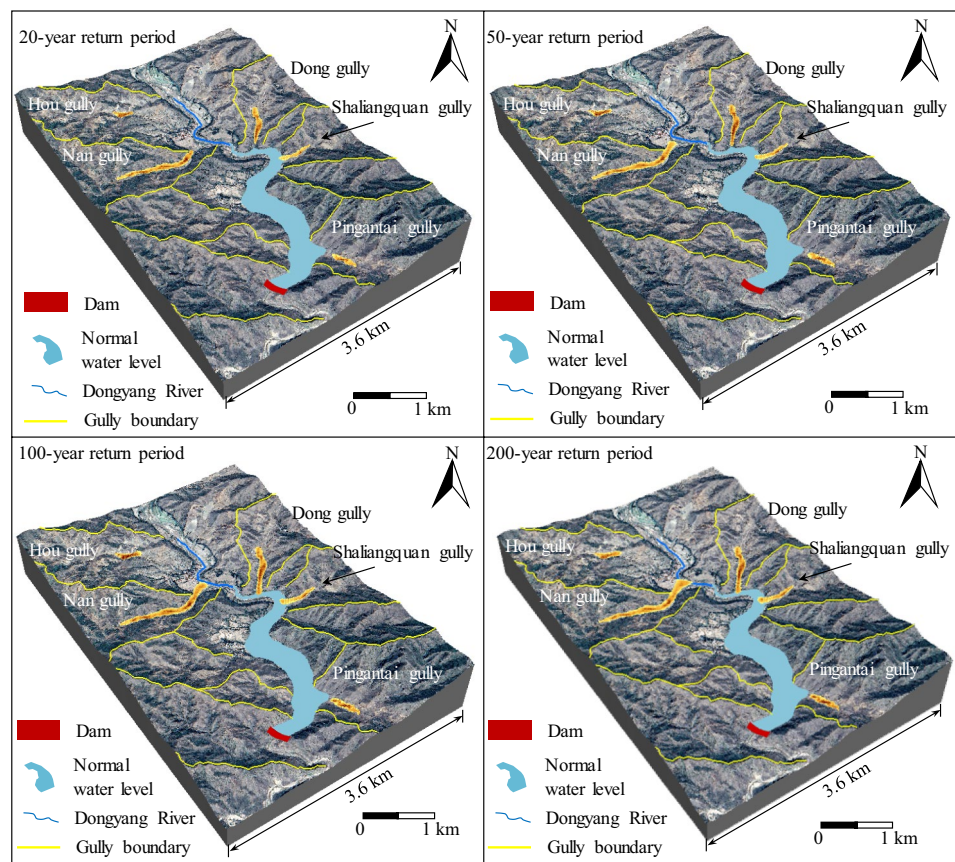
Fig. 16 Statistics of the simulated variables for the different frequency of debris flows. **a** Accumulation thickness. **b** Migration distance. **c** Affected range

Fig. 17 3D image map of the debris flow inflow reservoir of each gully in the study area under different rainfall frequencies

simulation results show that the parameters C_v and n have significant effects on the movement of debris flow (Fig. 19). The greater the C_v, the greater the viscosity of the debris flow, and the smaller the migration distance. The greater the value of n, the greater the frictional resistance, and the smaller the migration distance. Inspired by this, if the volume concentration of the debris flow and the roughness of the gully can be increased, the migration distance and scale of the debris flow will be effectively reduced, and the risk will be significantly reduced. Therefore, setting up drainage pipes and increasing vegetation coverage in the gully are economic and effective measures to prevent debris flow.

In addition, the SFLOW software used in this study is developed based on the finite volume shallow flow model. In order to test its effectiveness, Flo-2D, which has been widely recognized, has also been used to analyze the debris flow movement in Dong gully under different C_v and n values for 200-year return period (Fig. 20). The results show that the scale of the debris flow and the migration distance when C_v and n take different values are similar to the results of SFLOW analysis. But SFLOW can maintain good stability and higher efficiency in debris flow calculation under complex terrain conditions. This is mainly attributed to three aspects (Liang et al. 2009; Han et al. 2017): (1) SFLOW
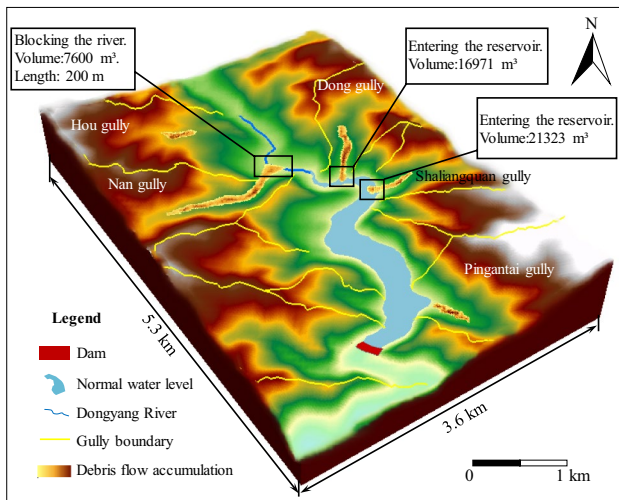
Fig. 18 The impact of debris flow on the reservoir for the 200-year return period

only searches for the wet meshes and adjacent dry meshes in each time step during the computation (Fig. 21), while the Flo-2D model based on the finite difference method needs to search all the meshes. (2) The step size of each time step in SFLOW can be set larger than FLo-2D. (3) The HLLC Riemann solver can well ensure the work of the model over highly irregular topography at a steady state. In conclusion, the application of SFLOW in debris flow assessment and prediction is of great significance for debris flow prevention in the project area, and can provide certain reference for similar projects.

However, the shallow water model (SFLOW) based on the theory of continuum mechanics cannot add mechanical boundaries and is only suitable for problems where the plane scale is much larger than the vertical scale. This means that the model can only analyze the movement characteristics of the surface fluid under gravity. Relevant information such as stress, strain, and features of material separation in the

Table 8 Classification of n and C_v

Level	Volume concentration C_v			Manning coefficient n		
	Low	Medium	High	Low	Medium	High
Value	0.15	0.35	0.55	0.02	0.15	0.8

Fig. 19 The flow depth corresponding to different n and C_v values. **a** $n=0.02$. **b** $n=0.15$. **c** $n=0.8$. **d** $C_v=0.15$. **e** $C_v=0.35$. **f** $C_v=0.55$
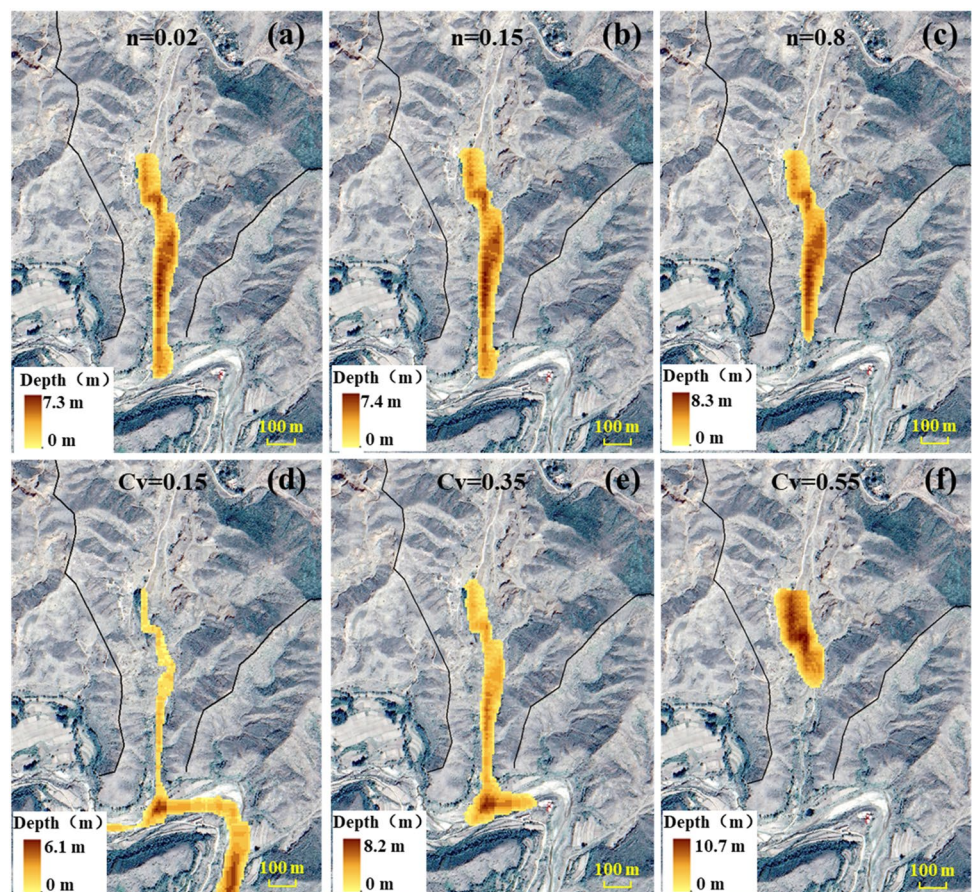
Fig. 20 The flow depth corresponding to different n and C_v values obtained by FLO-2D software. **a** $n=0.02$. **b** $n=0.15$. **c** $n=0.8$. **d** $C_v=0.15$. **e** $C_v=0.35$. **f** $C_v=0.55$
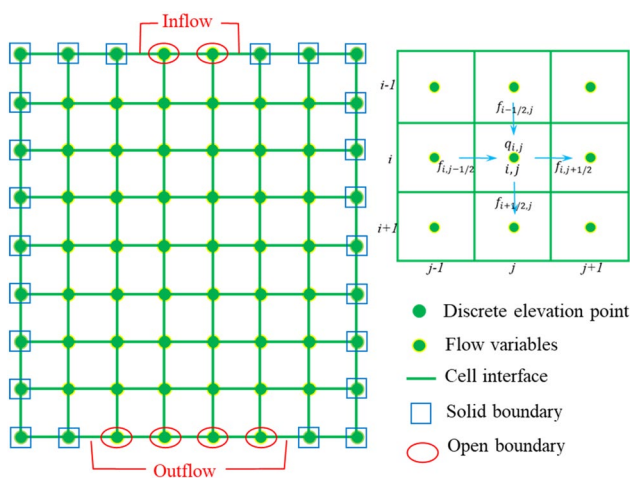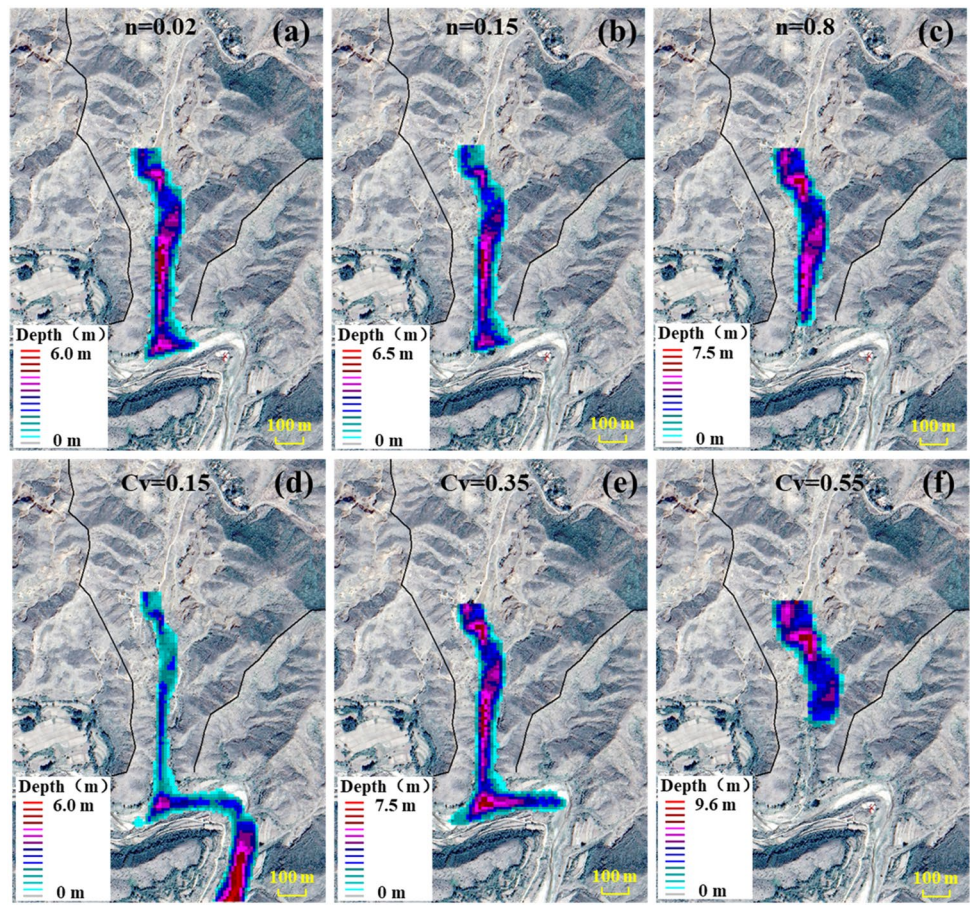

Fig. 21 Schematic of numerical computation domain and computation grid

Conclusion

Taking the pumped storage power station as an example, the neural network model and the shallow water flow model based on finite volume were used to evaluate the risk of debris flow and predict the hazard range. The results show that the increase in the affected area as well as the run-out distance with debris flows frequency decrease is non-linear, and extremely low-frequency debris flows are highly likely to cause more damage. It is estimated that 45,894 m^3 debris flow will enter the reservoir area for the 200-year return period. However, due to enough space reserved in the reservoir, this threat is limited and will not cause fatal damage to the reservoir area. In addition, parameter sensitivity analysis shows that volume concentration (C_v) and Manning coefficient (n) have significant effects on debris flow. Debris flow can be effectively prevented and controlled by increasing C_v and n values, such as setting drainage pipes or increasing vegetation coverage. In a word, the shallow water flow model based on limited volume can scientifically and effectively solve debris flow simulation and prediction problems under consideration of complex terrain, bottom friction, dry and wet control, etc., while ensuring the accuracy and high efficiency

dynamic process cannot be obtained. The above are the limitations of the model. With the continuous development of computer technology and numerical models, methods such as computational fluid dynamics (CFD) and multi-field coupling will inject new vitality into debris flow research.

of calculations, so as to achieve disaster prevention and engineering design requirements.

References

Bao YD, Sun XH, Chen JP, Zhang W, Han XD, Zhan JW (2019a) Stability assessment and dynamic analysis of a large iron mine waste dump in Panzhihua, Sichuan China. Environ Earth Sci 78:48

Bao YD, Chen JP, Sun XH, Han XD, Li YC, Zhang YW, Gu FF, Wang JQ (2019b) Debris flow prediction and prevention in reservoir area based on finite volume type shallow-water model: a case study of pumped-storage hydroelectric power station site in Yi County Hebei. China. Environ Earth Sci 78:19

Bout B, Lombardo L, Van Westen CJ, Jetten VG (2018) Integration of two-phase solid fluid equations in a catchment model for flash-floods, debris flows and shallow slope failures. Environ Model Softw 105:1–16

Chang FJ, Tseng KY, Chaves P (2007) Shared near neighbours neural network model: a debris flow. Hydrol Process 21:1968–1976

Chang M, Tang C, Van Asch ThWJ, Cai F (2017) Hazard assessment of debris flows in the Wenchuan earthquake-stricken area South West, China. Landslides 14(5):1783–1792

Chen HX, Zhang LM, Zhang S, Xiang B, Wang XF (2013) Hybrid simulation of the initiation and runout characteristics of a catastrophic debris flow. J Mt Sci 10(2):219–232

Chen YL, Qiu ZF, Li B, Yang ZJ (2018) Numerical simulation on the dynamic characteristics of a tremendous debris flow in Sichuan China. Processes 6(8):109

Dong JJ, Lee CT, Tung YH, Liu CN, Lin KP, Lee JF (2009) The role of the sediment budget in understanding debris flow susceptibility. Earth Surf Proc Land 34(12):1612–1624

Gentile F, Bisantino T, Trisorio Liuzzi G (2007) Debris-flow risk analysis in south Gargano watersheds (Southern-Italy). Nat Hazards 44(1):1–17

Han GQ, Wang D (1996) Numerical modeling of Anhui debris flow. J Hydr Engr, ASCE 122(5):262–265

Han XD, Chen JP, Xu PH, Zhan JW (2017) A well-balanced numerical scheme for debris flow run-out prediction in Xiaojia Gully considering different hydrological designs. Landslides 14(6):2105–2114

Han XD, Chen JP, Xu PH, Niu CC, Zhan JW (2018) Runout analysis of a potential debris flow in the Dongwopu gully based on a wellbalanced numerical model over complex topography. Bull Eng Geol Environ 77(2):679–689

Huang Y, Cheng HL, Dai ZL, Xu Q, Liu F, Sawada K, Moriguchi S, Yashima A (2014) SPH-based numerical simulation of catastrophic debris flows after the 2008 Wenchuan earthquake. Bull Eng Geol Env 74(4):1137–1151

Lai XJ, Li CS, Guo WC, Xu YH, Li YG (2019) Stability and dynamic characteristics of the nonlinear coupling system of hydropower station and power grid. Commun Nonlinear Sci Numer Simul 79:104919

Lee S, Ryu JH, Min K, Won JS (2003) Landslide susceptibility analysis using GIS and artificial neural network. Earth Surf Proc Land 28(12):1361–1376

Liang Q, Borthwick AGL (2009) Adaptive quadtree simulation of shallow flows with wet–dry fronts over complex topography. Comput Fluids 38(2):221–234

Liang WJ, Zhuang DF, Jiang D, Pan JJ, Ren HY (2012) Assessment of debris flow hazards using a Bayesian Network. Geomorphology 171–172:94–100

Lin ML, Wang KL, Huang GJ (2001) Simulation and analysis of debris flow of chui-sue river watershed. In: Proceedings of the Third International Conference on Watershed Management, pp 69–79

Lin PS, Lin JY, Hung JC, Yang MD (2002) Assessing debris-flow hazard in a watershed in Taiwan. Eng Geol 66(3–4):295–313

Lin ML, Wang KL, Huang JJ (2005) Debris flow run off simulation and verification case study of Chen-you-lan watershed Taiwan. Nat Hazards Earth Syst Sci 5:439–445

Liu XL (2002) Research progress on regional debris flow risk assessment. Chin J Geol Hazard Control 13(4):1–9. https://doi.org/10.3969/j.issn.1003-8035.2002.04.001 (**in Chinese**)

Liu XL, Tang C (1995) Risk assessment of debris flow. Science Press, Beijing (**in Chinese**)

Liu Y, Guo HC, Zou R, Wang LJ (2005) Neural network modeling for regional hazard assessment of debris flow in Lake Qionghai Watershed China. Environ Geol 49(7):968–976

Meng XN, Wang YQ (2015) Modelling and numerical simulation of two-phase debris flows. Acta Geotech 11(5):1027–1045

Ni HY, Zheng WM, Liu XL, Gao YC (2011) Fractal-statistical analysis of grainsize distributions of debris-flow deposits and its geological implications. Landslides 8(2):253–259

O'Brien JS (2006) FLO-2D User's manual. FLO-2D Software Inc, Nutrioso

Ouyang CJ, He SM, Xu Q, Luo Y, Zhang WC (2013) A MacCormack-TVD finite difference method to simulate the mass flow in mountainous terrain with variable computational domain. Comput Geosci 52:1–10

Regmi NR, Giardino JR, McDonald EV, Vitek JD (2013) A comparison of logistic regression-based models of susceptibility to landslides in western Colorado, USA. Landslides 11(2):247–262

Specification of geological investigation for debris flow stabilization DZ/T0220-2006 (2006) Issued by the Ministry of land and resources of the people's Republic of China

Sun XH, Chen JP, Bao YD, Han XD, Zhan JW, Peng W (2018) Landslide susceptibility mapping using logistic regression analysis along the Jinsha River and its tributaries close to Derong and Deqin County, southwestern China. ISPRS Int J Geo Inform. https://doi.org/10.3390/ijgi7110438

Sun XH, Chen JP, Han XD, Bao YD, Zhan JW, Peng W (2020) Application of a GIS-based slope unit method for landslide susceptibility mapping along the rapidly uplifting section of the upper Jinsha River, South-Western China. Bull Eng Geol Env 79:533–549. https://doi.org/10.1007/s10064-019-01572-5

Tien Bui D, Pradhan B, Lofman O, Revhaug I, Dick OB (2012) Landslide susceptibility assessment in the Hoa Binh province of Vietnam: a comparison of the Levenberg–Marquardt and Bayesian regularized neural networks. Geomorphology 171–172:12–29

Tunusluoglu MC, Gokceoglu C, Nefeslioglu HA, Sonmez H (2007) Extraction of potential debris source areas by logistic regression technique: a case study from Barla, Besparmak and Kapi mountains (NW Taurids, Turkey). Environ Geol 54(1):9–22

Valero A, Valero A (2010) Physical geonomics: Combining the exergy and Hubbert peak analysis for predicting mineral resources depletion. Resour Conserv Recycl 54(12):1074–1083

Wang XK, Huang E, Cui P (2003) Simulation and prediction of debris flow using artificial neural network. Chin Geogr Sci 13(3):262–266

Wang W, Chen GQ, Han Z, Zhou SH, Zhang H, Jing PD (2016b) 3D numerical simulation of debris-flow motion using SPH method incorporating non-Newtonian fluid behavior. Nat Hazards 81(3):1981–1998

Wang CM, Tian SW, Wang YH, Ruan YK, Ding GL (2016a) Risk assessment of debris flow: a method of SVM based on FCM. J Jinlin Univ Earth Sci Ed 46(4):1168–1175. https://doi.org/10.1378/j.cnki.jjuese.201604203 (**in Chinese**)

Wu YL, Li WP, Liu P, Bai HY, Wang QQ, He JH, Liu Y, Sun SS (2016) Application of analytic hierarchy process model for landslide susceptibility mapping in the Gangu County, Gansu Province China. Environ Earth Sci 75:5

Yu Q, Yan X, Wang Q, Yang T, Kong Y, Huang X et al (2020) X-ray computed tomography-based evaluation of the physical properties and compressibility of soil in a reclamation area. Geoderma 375:114524

Zhan JW, Chen JP, Zhang W, Han XD, Sun XH, Bao YD (2018) Mass movements along a rapidly uplifting river valley: an example from the upper Jinsha River, southeast margin of the Tibetan Plateau. Environ Earth Sci 77:18

Zhang SF, Andrews-Speed P, Perera P (2015) The evolving policy regime for pumped storage hydroelectricity in China: a key support for low-carbon energy. Appl Energy 150:15–24

Zhang X, Wu Y, Zhai E, Ye P (2020) Coupling analysis of the heat-water dynamics and frozen depth in a seasonally frozen zone. J Hydrol 593:125603